Bol. Soc. Paran. Mat.
©SPM – E-ISSN-2175-1188
SPM: www.spm.uem.br/bspm

(3s.) **v. 2025 (43)** : 1–18.
ISSN-0037-8712
doi:10.5269/bspm.76771

A physics-informed neural network approach to analyze the dynamics of SIR epidemic model with Hattaf fractional derivative

M. Ait Ichou[1], Z. Hajhouji[3] and K. Hattaf[2,3]

ABSTRACT: This paper presents a susceptible-infected-removed (SIR) model with the generalized Hattaf fractional derivative involving a non-singular kernel, integrated in a physics-informed neural networks (PINNs), as a means of comprehending the temporal evolution dynamics of infectious diseases. The proof demonstrates the existence, uniqueness, positivity and boundedness of the solution. This study establishes the stability of the disease-free equilibrium in the Mittag-Leffler sense. Another significant contribution of this work is the integration of PINNs approach to analyze the SIR model. We propose this approach as an alternative to classical numerical methods for solving the SIR model. Our results demonstrate that PINNs are a promising solution, not only for solving this type of system, but also for studying the dynamics of infectious diseases.

Key Words: SIR Model, Hattaf fractional derivative, Deep Learning, PINNs.

Contents

1. Introduction

Mathematical models of infectious diseases are purely theoretical tools that facilitate the study and analysis of the transmission dynamics of infectious diseases. The SIR model (Susceptible-Infected-removed) represents a foundational approach in the field of epidemiological modeling. It is one of the most straightforward mathematical models for studying the dissemination of a disease. The computational cost of solving the SIR model with a fractional derivative using a classical solution method is considerable when the step of discretization is small. Another category of approaches, namely PINNs, offers a considerably faster computation time than classical methods while maintaining exceptional prediction quality [1].

One particularly effective machine-learning algorithm for addressing spatial challenges is the neural network. The fundamental premise of this algorithm is the reduction of the loss function, which facilitates the enhancement of approximations for mathematical solutions. Neural networks have become the most efficient method for solving even the most challenging mathematical problems. The application of the neural network method to the solution of fractional differential equations has been the subject of considerable research activity, largely driven by the growing success of neural network techniques for solving ordinary differential equations (ODEs) and partial differential equations (PDEs) [2,3,4,5,6]. The principal objective of this study is to utilize neural networks for the resolution of the fractional equation.

The integration of physical information into neural networks has recently emerged as a topic of significant interest among the scientific community, largely due to the unique capabilities that these networks possess in terms of data and equation integration. Ren et al. [7] investigated the efficacy

Submitted May 12, 2025. Published August 24, 2025
2010 *Mathematics Subject Classification:* 92D30, 34A34, 37N25, 26A33, 68T07, 65M75.

of improved fractional physics-informed neural networks (IFPINNs) for solving fractional differential equations with time fractional orders between 1 and 2. Wang et al. [8] proposed a novel general PINN framework, designated as quasi Monte Carlo (GMC-PINNs), for the resolution of fractional partial differential equations (FPDEs) within irregular domains. This methodology has been enhanced through the introduction of nodes based on an ensemble probability density function, which facilitates their positioning in more concentrated regions in proximity to the points of differentiation. Barmparis and Tsironis [9] used physics-informed machine learning and a simple SIR model to discribe the dynamics of COVID-19 pandemic with social distancing measures. They considered time-dependent infection rates and neglected other factors like, immigration, vaccination, natality rate and death rate due to disease. In a study by [10], the authors proposed the use of PINNs for monitoring macular evolution. The employment of PINNs enables the monitoring of temporal variations in model parameters and state variables. Moreover, they have devised a streamlined approach for configuring PINNs to assess the system equations. The objective is to divide the training process into two stages: first, based on the epidemiological data; and then, based on the residual of the system equations. The system formulas are as follows: The proposed method is applied to five synthetic test cases and two real scenarios that reproduce the initial stages of the epidemic. In this regard, Hu et al. [11] applied a variant of a PINN and proposed a wavelet transform to process the data needed to train the network. They found that their modified network was capable of stable estimation and suggested the effectiveness of their modified PINN, particularly in the case of multiple unknown variables.

PINNs have emerged as a prevalent approach in machine learning for addressing inverse problems, as evidenced by the citations in references [12,13]. PINN models utilized in contemporary software frameworks offer a combination of simplicity and flexibility, enabling the same code to be applied with minimal modifications to investigate both direct and inverse problems. This contrasts with traditional inverse modeling methods, which often entailed a laborious and time-consuming process. In a study by Aghdaouia et al. [12], a fractional model of coronavirus disease was developed, including unreported cases. The model was estimated using the PINNs approach. In their study, Nguyen et al. [14] investigated the propagation of the SARS-CoV-2 virus in the presence of both interpersonal transmission and environmental contamination. It was put forth that the differential equation systems which characterize the dynamics of infectious diseases be solved using the PINN approach. The proposed PINN method is a promising approach for addressing these types of systems. In order to ascertain the suitability of the PINNs technique as a direct solver, an inverse solver, and a solver within the context of constrained data, a series of computer tests were conducted.

In this paper, we put forth a fractional model of SIR that incorporates the recently developed non-singular kernel fractional derivative. This paper presents a solution to the SIR model with a fractional derivative based on PINNs. We examine the suitability and impact of fractional operators on the model and employ a PINN-based methodology to estimate fractional orders.

The following is the paper's outline. We present the mathematical model and demonstrate the existence of fractional model solutions in Section 2. We report the stability of the endemic and disease-free equilibrium points in Section 3. In Section 4, we present the sensitivity analysis of our model. In Section 5, the PINNs method for treating infectious diseases, as described in this work, is introduced and its potential as a treatment modality is explored. Additionally, we carry out a range of computer tests to verify the effectiveness of the PINNs approach as an forward solver. In Section 6, we present a concise analysis followed by a conclusion.

2. The problem model and the existence of solution

This section presents a SIR model that describes the dynamics of disease using the recently developed non-singular kernel fractional derivative. Furthermore, the well-known fixed point theorem will be employed to demonstrate the existence and uniqueness of the solution to the suggested model.

The transmission dynamics of the novel coronavirus disease, also known as COVID-19, described by

the following differential equations:

$$\begin{cases} \mathcal{D}_{0,w}^{\iota,\theta} S(t) = \Lambda + \Upsilon - \mu S - h(S,I)I - \eta S, \\ \mathcal{D}_{0,w}^{\iota,\theta} I(t) = \rho + h(S,I)I - (\mu + \gamma + \xi)I, \\ \mathcal{D}_{0,w}^{\iota,\theta} R(t) = \xi I + \eta S - \mu R, \end{cases} \tag{2.1}$$

where the rate of recruitment of susceptible individuals is Λ, and the rate of infection acquired via effective contact with infected individuals is $h(S,I)I = \dfrac{\sigma S}{1+kI} I$. μ represents the natural death rate for all classes, and γ represents the death rate due to disease. The parameters ξ and η represent the recovery rate of infected individuals and the vaccination rate, respectively. Lastly, the immigrant to susceptible and the immigrant to infected are represented by Υ and ρ, respectively.

In this context, the operator $\mathcal{D}_{0,w}^{\iota,\theta}$ is used to denote the generalized Hattaf fractional (GHF) derivative [15], which is defined with respect to the weight $w(t)$ for any given function $f(t)$, as follows:

$$\mathcal{D}_{0,w}^{\iota,\theta} f(t) = \frac{\mathcal{GHF}(\iota)}{1-\iota} \frac{1}{w(t)} \int_0^t E_\theta \left[-\mu_\iota (t-z)^\theta \right] \frac{d}{dz}(wf)(x) dz, \tag{2.2}$$

where $w \in \mathcal{C}^1(a,b)$, $w > 0$ on $[a,b]$, $\mu_\iota = \frac{\iota}{1-\iota}$, $\mathcal{GHF}(\iota)$ is a normalization function that satisfies $\mathcal{GHF}(0) = \mathcal{GHF}(1) = 1$ and $E_\theta(t) = \displaystyle\sum_{k=0}^{+\infty} \frac{t^k}{\Gamma(\theta k + 1)}$ is the Mittag-Leffler function of parameter θ. It is important to note that (2.1) extends the ODE model introduced in [16]. Also, the GHF derivative is a non-local operator and it generalizes well-known fractional derivatives with non-singular kernels like Caputo-Fabrizio [17] and Atangana-Baleanu [18] fractional operators.

Lemma 2.1 *The closed set* $\Gamma = \left\{ (S,I,R) \in \mathbb{R}_+^3 : S + I + R \leq \frac{\lambda}{\mu} \right\}$ *is positively invariant for the GHF fractional model (2.1).*

Proof: Let $\mathcal{N}(t) = S(t) + I(t) + R(t)$.
The addition of all equations within the system, as referenced in equation (2.1), yields the following result:

$$\begin{aligned} \mathcal{D}_{0,w}^{\iota,\theta} \mathcal{N}(t) &= \Lambda + \Upsilon + \rho - \mu \mathcal{N}(t) - \gamma I \\ &\leq \lambda - \mu \mathcal{N}(t), \end{aligned}$$

where $\lambda = \Lambda + \Upsilon + \rho$. Then there exists a nonnegative function $u(t)$ such that

$$\mathcal{D}_{0,w}^{\iota,\theta} \mathcal{N}(t) = \lambda - \mu \mathcal{N}(t) - u(t).$$

In accordance with Lemma 2 of [19], we have

$$\begin{aligned} \mathcal{N}(t) =& \frac{\mathcal{GHF}(\iota) w(0)}{J(\iota) w(t)} \left(\mathcal{N}(0) - \frac{\lambda}{\mu} \right) E_\theta \left(-\frac{\alpha\mu}{J(\iota)} t^\theta \right) + \frac{\lambda}{\mu} \\ &- \frac{\lambda \mathcal{GHF}(\alpha)}{\mu J(\iota)} E_\theta \left(-\frac{\alpha\mu}{J(\iota) w(t)} t^\theta \right) * w' - \frac{\mu(1-\alpha)}{J(\iota)} \\ &- \frac{\iota\theta \mathcal{GHF}(\iota)}{J^2(\alpha) w(t)} t^{\theta-1} E_{\theta,\theta+1}^2 \left(-\frac{\iota\mu}{J(\iota)} t^\theta \right) * (wu), \end{aligned}$$

where $J(\iota) = \mathcal{GHF}(\iota) + \mu(1-\iota)$. Hence,

$$\mathcal{N}(t) \leq \frac{\mathcal{GHF}(\iota) w(0)}{J(\iota) w(t)} \left(\mathcal{N}(0) - \frac{\lambda}{\mu} \right) E_\theta \left(-\frac{\iota\mu}{J(\iota)} t^\theta \right) + \frac{\lambda}{\mu}.$$

If $\mathcal{N}(0) \leq \frac{\lambda}{\mu}$, then $\mathcal{N}(t) \leq \frac{\lambda}{\mu}$. This completes the proof. □

Next, we'll attempt to use the well-known fixed point theorem to demonstrate the existence and uniqueness of the solution for the suggested model. Let $\mathcal{J} = [0, b]$ and $\mathcal{C}(\mathcal{J})$ be the Banach space of continuous functions from $\mathcal{J}$ to $\mathbb{R}$. Let $\mathbb{G} = (\mathcal{C}(\mathcal{J}))^3$ be the space with the norm $\|(S, I, R)\| = \|S\| + \|I\| + \|R\|$, where $\|I\| = \sup_{t\in\mathcal{J}} |I(t)|$, $\|R\| = \sup_{t\in\mathcal{J}} |R(t)|$ and $\|S\| = \sup_{t\in\mathcal{J}} |S(t)|$. The considered model can be written as

$$\begin{cases} \mathcal{D}_{0,w}^{\iota,\theta} S(t) = G_1(t, S), \\ \mathcal{D}_{0,w}^{\iota,\theta} I(t) = G_2(t, I), \\ \mathcal{D}_{0,w}^{\iota,\theta} R(t) = G_3(t, R), \end{cases} \tag{2.3}$$

where

$$G_1(t, S) = \Lambda + \Upsilon - \mu S - h(S, I)I - \eta S,$$

$$G_2(t, I) = \rho + h(S, I)I - (\mu + \gamma + \xi)I,$$

$$G_3(t, R) = \xi I + \eta S - \mu R.$$

Employing the generalized fractional integral operator $\mathcal{J}_{0,w}^{\iota,\theta}$ [15] corresponding to $\mathcal{D}_{0,w}^{\iota,\theta}$ on both-sides of (2.3), we have

$$\begin{aligned} S(t) - \frac{w(0)}{w(t)} S(0) &= \frac{1-\iota}{\mathcal{GHF}(\iota)} G_1(t, S) + \frac{\iota}{w(t)\Gamma(\theta)\mathcal{GHF}(\iota)} \int_0^t (t-z)^{\theta-1} w(z) G_1(z, S) dz, \\ I(t) - \frac{w(0)}{w(t)} I(0) &= \frac{1-\iota}{\mathcal{GHF}(\iota)} G_2(t, I) + \frac{\iota}{w(t)\Gamma(\theta)\mathcal{GHF}(\iota)} \int_0^t (t-z)^{\theta-1} w(z) G_2(z, I) dz, \\ R(t) - \frac{w(0)}{w(t)} R(0) &= \frac{1-\iota}{\mathcal{GHF}(\iota)} G_3(t, R) + \frac{\iota}{w(t)\Gamma(\theta)\mathcal{GHF}(\iota)} \int_0^t (t-z)^{\theta-1} w(z) G_3(z, R) dz. \end{aligned}$$

It can be demonstrated that if the functions $S(t)$, $I(t)$, and $R(t)$ are subject to upper bounds, then it is only in this context that the functions G_1, G_2, and G_3 satisfy the Lipschitz condition. In addition, we have

$$\begin{aligned} |G_1(t, S) - G_1(t, S^*)| &\leq L_1 |S(t) - S^*(t)|, \\ |G_2(t, I) - G_2(t, I^*)| &\leq L_2 |I(t) - I^*(t)|, \\ |G_3(t, R) - G_3(t, R^*)| &\leq L_3 |R(t) - R^*(t)|, \end{aligned} \tag{2.4}$$

where

$$\begin{aligned} L_1 &= \mu + \eta + \frac{\sigma}{k}, \\ L_2 &= \frac{\sigma\lambda}{\mu} + \mu + \gamma + \xi, \\ L_3 &= \mu. \end{aligned}$$

This indicates that each of the three functions has been addressed by the Lipschitz condition. Nevertheless, the recursive formula yields the following result:

$$\begin{aligned} S_p(t) - \frac{w(0)}{w(t)} S(0) &= \frac{1-\iota}{\mathcal{GHF}(\iota)} G_1(t, S_{p-1}) + \frac{\iota}{w(t)\Gamma(\theta)\mathcal{GHF}(\iota)} \int_0^t (t-z)^{\theta-1} w(z) G_1(z, S_{p-1}) dz \\ I_p(t) - \frac{w(0)}{w(t)} I(0) &= \frac{1-\iota}{\mathcal{GHF}(\iota)} G_2(t, I_{p-1}) + \frac{\iota}{w(t)\Gamma(\theta)\mathcal{GHF}(\iota)} \int_0^t (t-z)^{\theta-1} w(z) G_2(z, I_{p-1}) dz \\ R_p(t) - \frac{w(0)}{w(t)} R(0) &= \frac{1-\iota}{\mathcal{GHF}(\iota)} G_3(t, R_{p-1}) + \frac{\iota}{w(t)\Gamma(\theta)\mathcal{GHF}(\iota)} \int_0^t (t-z)^{\theta-1} w(z) G_3(z, R_{p-1}) dz \end{aligned} \tag{2.5}$$

By considering the difference between successive terms, the following results are obtained.

$$\begin{aligned}
\Phi_{S,p}(t) &= S_p(t) - S_{p-1}(t) \\
&= \frac{1-\iota}{\mathcal{GHF}(\iota)} \left(G_1\left(t, S_{p-1}\right) - G_1\left(t, S_{p-2}\right)\right) \\
&\quad + \frac{\iota}{w(t)\Gamma(\theta)\mathcal{GHF}(\iota)} \int_0^t (t-z)^{\theta-1} w(z) \left(G_1\left(z, S_{p-1}\right) - G_1\left(z, S_{p-2}\right)\right) dz, \\
\Phi_{I,p}(t) &= I_p(t) - I_{p-1}(t) \\
&= \frac{1-\iota}{\mathcal{GHF}(\iota)} \left(G_2\left(t, I_{p-1}\right) - G_2\left(t, I_{p-2}\right)\right) \\
&\quad + \frac{\iota}{w(t)\Gamma(\theta)\mathcal{GHF}(\iota)} \int_0^t (t-z)^{\theta-1} w(z) \left(G_2\left(z, I_{p-1}\right) - G_2\left(z, I_{p-2}\right)\right) dz, \\
\Phi_{R,p}(t) &= R_p(t) - R_{p-1}(t) \\
&= \frac{1-\iota}{\mathcal{GHF}(\iota)} \left(G_3\left(t, R_{p-1}\right) - G_3\left(t, R_{p-2}\right)\right) \\
&\quad + \frac{\iota}{w(t)\Gamma(\theta)\mathcal{GHF}(\iota)} \int_0^t (t-z)^{\theta-1} w(z) \left(G_3\left(z, R_{p-1}\right) - G_3\left(z, R_{p-2}\right)\right) dz.
\end{aligned}$$

Then

$$\begin{aligned}
|\Phi_{S,p}(t)| \leq & \frac{1-\iota}{\mathcal{GHF}(\iota)} L_1 |\Phi_{S,p-1}(t)| \\
& + \frac{\iota L_1}{w(t)\Gamma(\theta)\mathcal{GHF}(\iota)} \int_0^t (t-z)^{\theta-1} w(z) |\Phi_{S,p-1}(t)| dz \\
|\Phi_{I,p}(t)| \leq & \frac{1-\iota}{\mathcal{GHF}(\iota)} L_2 |\Phi_{I,p-1}(t)| \\
& + \frac{\iota L_2}{w(t)\Gamma(\theta)\mathcal{GHF}(\iota)} \int_0^t (t-z)^{\theta-1} w(z) |\Phi_{I,p-1}(t)| dz \\
|\Phi_{R,p}(t)| \leq & \frac{1-\iota}{\mathcal{GHF}(\iota)} L_3 |\Phi_{R,p-1}(t)| \\
& + \frac{\iota L_3}{w(t)\Gamma(\theta)\mathcal{GHF}(\iota)} \int_0^t (t-z)^{\theta-1} w(z) |\Phi_{R,p-1}(t)| dz
\end{aligned} \tag{2.6}$$

Theorem 2.1 *Assume that* $L_i \left(\frac{1-\iota}{\mathcal{GHF}(\iota)} + \frac{\iota b^\theta}{\theta\Gamma(\theta)\mathcal{GHF}(\iota)} \right) < 1$ *is satisfied for each* $i = 1, 2, 3$. *Then system (2.1) with non-negative initial conditions has a unique solution on the interval* $[0, b]$.

Proof: As indicated by Lemma 2.1, the functions $S(t)$, $I(t)$ and $R(t)$ are all bounded. Furthermore, the symbols G_1, G_2 and G_3 satisfy the Lipschitz condition, as can be seen with regard to equation (2.4). Consequently, the application of equation (2.6) in conjunction with the recursive hypothesis yields the following result:

$$\begin{aligned}
\|\Phi_{S,p}\| &\leq \left(L_1 \frac{1-\iota}{\mathcal{GHF}(\iota)} + \frac{\iota L_1 b^\theta}{\theta\Gamma(\theta)\mathcal{GHF}(\iota)} \right)^{p-1} \|S_1 - S_0\|, \\
\|\Phi_{I,p}\| &\leq \left(L_2 \frac{1-\iota}{\mathcal{GHF}(\iota)} + \frac{\iota L_2 b^\theta}{\theta\Gamma(\theta)\mathcal{GHF}(\iota)} \right)^{p-1} \|I_1 - I_0\|, \\
\|\Phi_{R,p}\| &\leq \left(L_3 \frac{1-\iota}{\mathcal{GHF}(\iota)} + \frac{\iota L_3 b^\theta}{\theta\Gamma(\theta)\mathcal{GHF}(\iota)} \right)^{p-1} \|R_1 - R_0\|.
\end{aligned} \tag{2.7}$$

As a consequence, as p approaches infinity, the aforementioned sequences satisfy the conditions that result in the following limits: Furthermore, the triangle inequality can be applied to each value of q, and using

equation (2.7), the result is

$$\|S_{p+q}(t) - S_p(t)\| \leq \sum_{j=p+1}^{p+q} \mathcal{U}_1^j = \frac{\mathcal{U}_1^{p+1} - \mathcal{U}_1^{p+q+1}}{1-\mathcal{U}_1},$$
$$\|I_{p+q}(t) - I_p(t)\| \leq \sum_{j=p+1}^{p+q} \mathcal{U}_2^j = \frac{\mathcal{U}_2^{p+1} - \mathcal{U}_2^{p+q+1}}{1-\mathcal{U}_2},$$
$$\|R_{p+q}(t) - R_p(t)\| \leq \sum_{j=p+1}^{p+q} \mathcal{U}_3^j = \frac{\mathcal{U}_3^{p+1} - \mathcal{U}_3^{p+q+1}}{1-\mathcal{U}_3},$$

with $\mathcal{U}_i = L_i \frac{1-\iota}{\mathcal{GHF}(\iota)} + \frac{\iota L_i b^\theta}{\theta\Gamma(\theta)\mathcal{GHF}(\iota)}$. Thus, we conclude that the sequences S_p, I_p, R_p are described as Cauchy sequences. As a result, they converge evenly [20]. Furthermore, the limit of these sequences when $p \to \infty$ is the only solution of the model may be found by applying the limit theorem to all of the equations in (2.5). □

In the case of no immigration of infected individuals (i.e. $\rho = 0$), the proposed model always has a disease-free equilibrium point denoted by $\mathcal{P}_0\,(S_0, 0, 0)$, where $S_0 = \frac{\Lambda+\Upsilon}{\mu+\eta}$. Thus, the following expression yields the basic reproduction number $\mathcal{R}_0$:

$$\mathcal{R}_0 = \frac{h(\frac{\Lambda+\Upsilon}{\mu+\eta}, 0)}{\mu+\gamma+\xi} = \frac{\sigma(\Lambda+\Upsilon)}{(\mu+\eta)(\mu+\gamma+\xi)}.$$

The number represents the typical number of secondary infections that an infected individual throughout his infectious period causes.

However, the model also features an additional equilibrium point known as the endemic equilibrium point, which is indicated by $\mathcal{P}_1\,(S_1, I_1, R_1)$, where

$$S_1 = \frac{\rho+\Lambda+\Upsilon-(\mu+\gamma+\xi)I_1}{\mu+\eta},$$
$$I_1 = \frac{[\rho(\mu+\eta)k + \sigma(\rho+\Lambda+\Upsilon) - (\mu+\gamma+\xi)(\mu+\eta)] + \sqrt{\triangle}}{2\,[\sigma(\rho+\Lambda+\Upsilon) + (\rho+\Lambda+\Upsilon)(\mu+\eta)k]},$$
$$R_1 = \frac{\xi I_1 + \eta S_1}{\mu},$$

where

$$\triangle = [\rho(\mu+\eta)k + \sigma(\rho+\Lambda+\Upsilon) - (\mu+\gamma+\xi)(\mu+\eta)]^2 + 4\,[\sigma(\rho+\Lambda+\Upsilon) + (\rho+\Lambda+\Upsilon)(\mu+\eta)k]\,\rho(\mu+\eta).$$

3. Stability analysis

In this section, we study the Mittag-Leffler stability of the disease-free equilibrium point of the proposed model.

Theorem 3.1 *The model (2.1) is Mittag-Leffler stable when $\mathcal{R}_0 < 1$ and $\rho = 0$.*

Proof: Consider the following Lyapunov function

$$L(S, I) = \omega(S_0 - S) + I,$$

where $\omega = \dfrac{1-\mathcal{R}_0}{2\mathcal{R}_0}$ and L is a candidate Lyapunov function. We have $L\,(\mathcal{P}_0) = 0$ and $L(X) > 0$ for all $X \neq \mathcal{P}_0$. In addition

$$\mathcal{D}_{0,w}^{\iota,\theta} L(S, I) = -\omega \mathcal{D}_{0,w}^{\iota,\theta} S + \mathcal{D}_{0,w}^{\iota,\theta} I$$
$$= (\mu+\eta)(S - S_0) + 2\frac{\sigma SI}{1+kI} - (\mu+\gamma+\xi)I.$$

Since $S \leq S_0$, we have

$$\begin{aligned}
\mathcal{D}_{0,w}^{\iota,\theta} L(S,I) &\leq -\omega(\mu+\eta)(S_0-S) + (1+\omega)h(S_0,0)I - (\mu+\gamma+\xi)I, \\
&\leq -\omega(\mu+\eta)(S_0-S) + \big((1+\omega)\mathcal{R}_0 - 1\big)I, \\
&\leq -\omega(\mu+\eta)(S_0-S) - \frac{1}{2}\big(1-\mathcal{R}_0\big)I, \\
&\leq -\phi L(S,I),
\end{aligned}$$

where $\phi = \min\{\mu+\eta, \frac{1}{2}\big(1-\mathcal{R}_0\big)\}$. This inequality holds if $\mathcal{R}_0 < 1$.
By applying Theorem 4 of [21], we conclude that the disease-free equilibrium $\mathcal{P}_0$ is Mittag-Leffler stable. □

Biologically, Theorem 3.1 means that the disease will die out if there is no immigration of infected individuals and the basic reproduction number is less than one.

4. Sensitivity analysis

Sensitivity analysis is a fundamental step in the modeling process. It enables us to understand the impact of changes in model parameters on observed dynamics. More specifically, with regard to the model studied in this research, the sensitivity analysis focuses mainly on the basic reproduction number given by:

$$\mathcal{R}_0 = \frac{\sigma(\Lambda+\Upsilon)}{(\mu+\eta)(\mu+\gamma+\xi)}$$

which is a key indicator for understanding the transmission and immigration of COVID-19 infection.

To assess the influence of each parameter on $\mathcal{R}_0$, we use the normalized sensitivity index, defined for a ϖ parameter by:

$$IN_{\varpi} = \frac{\partial \mathcal{R}_0}{\partial \varpi} \times \frac{\varpi}{\mathcal{R}_0} \tag{4.1}$$

This index measures the relative variation in $\mathcal{R}_0$ in response to a relative variation in the parameter ϖ. Applying formula (4.1) to all the parameters of system (2.1), we obtain:

- For the σ transmission rate:
$$IN_{\sigma} = 1,$$
indicating that $\mathcal{R}_0$ is linearly proportional to σ.

- For the recruitment rate Λ and the immigration rate of susceptible Υ:
$$IN_{\Lambda} = \frac{\Lambda}{\Lambda+\Upsilon} \;\; ; \;\; IN_{\Upsilon} = \frac{\Upsilon}{\Lambda+\Upsilon},$$
which means that an increase in these parameters leads to a proportional increase in $\mathcal{R}_0$.

- For the μ natural mortality rate:
$$IN_{\mu} = -\left(\frac{\mu(2\mu+\gamma+\xi+\eta)}{(\mu+\eta)(\mu+\gamma+\xi)}\right),$$
suggesting that increasing μ reduces $\mathcal{R}_0$.

- For the η vaccination rate:

$$IN_\eta = -\frac{\eta}{\mu+\eta}$$

showing that vaccination helps reduce $\mathcal{R}_0$.

- For the mortality rate due to disease γ :

$$IN_\gamma = -\frac{\gamma}{\mu+\gamma+\xi},$$

and for the cure rate ξ:

$$IN_\xi = -\frac{\xi}{\mu+\gamma+\xi},$$

indicating that high cure or mortality rates reduce $\mathcal{R}_0$.

Sensitivity measurements for the various parameters are shown in figure 1 and summarized in table 1. From Table 1 we can see that the parameters most sensitive to the number of basic reproductions $\mathcal{R}_0$

Table 1: Sensitivity index of R_0.

Parameter	Sensitivity index	Effect of a 10% increase on $\mathcal{R}_0$.
σ	1	+10%
Λ	0.83	+8.3%
Υ	0.16	+1.6%
μ	−0.83	−8.3%
η	−0.5	−5%
γ	−0.33	−3.3%
ξ	−0.33	−3.3%

in the SIR model are σ and Λ clearly, an increase in the value of one of these parameters will increase the basic reproduction number. On the other hand, an increase in the value of the other parameters μ and η will lead to a decrease in Ro. We obtain the following results, illustrated in Figures 1 and 2.

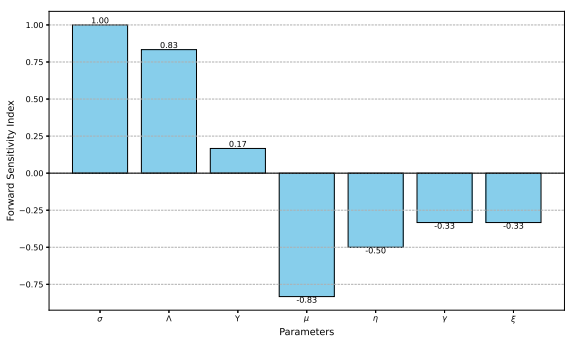

Figure 1: Forward sensitivity analysis to evaluate the impact of the parameters on $\mathcal{R}_0$.

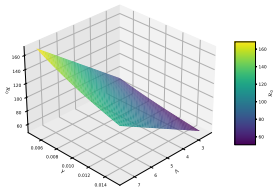

(a) $\mathcal{R}_0$ versus the parameters Λ and γ.

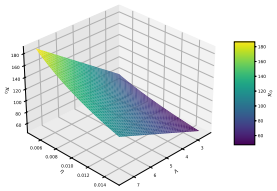

(b) $\mathcal{R}_0$ versus the parameters Λ and η.

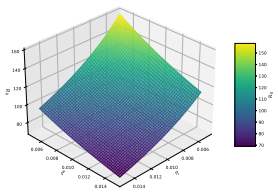

(c) $\mathcal{R}_0$ versus the parameters ξ and η.

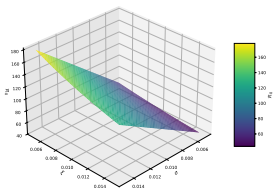

(d) $\mathcal{R}_0$ versus the parameters ξ and σ.

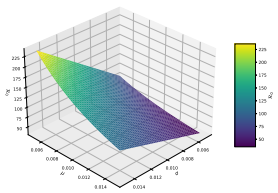

(e) $\mathcal{R}_0$ versus the parameters Λ and γ.

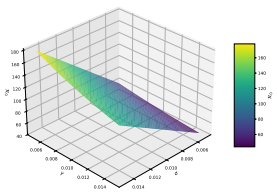

(f) $\mathcal{R}_0$ versus the parameters μ and σ.

Figure 2: Impact of various parameters for model (2.1) on behavior of $\mathcal{R}_0$.

5. PINNs approach for solving SIR model

PINNs are deep learning-based techniques for PDEs that describe multi-physics phenomena, including ordinary and partial differential, integrodifferential, and fractional order operators [22,23,24]. One of the key factors contributing to the success of these deep learning methods is the incorporation of neural networks, which are systems designed to emulate the decision-making processes observed in the human brain.

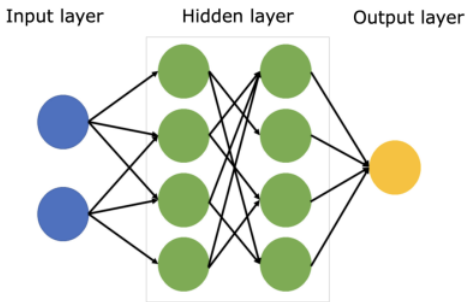

Figure 3: Illustration of a neural network.

In what follows, we propose, based on recent PINN developments [14], to use the hidden physics of infectious diseases (i.e. system (2.1)) and deduce the latent quantities of interest (i.e. S, I and R) by approximating them using deep neural networks. Contemporary techniques for solving forward and backward problems related to differential equations are behind this decision, where the unknown solution is approximated either by a neural network or by a Gaussian process. Using these methods, we approximate the latent function $t \mapsto (S, I, R)$ using a deep neural network and obtain the following physics-aware neural networks (see, Figure 4):

$$E_1 := \mathcal{D}_{0,w}^{\iota,\theta} S(t) - \Lambda - \Upsilon + \mu S + h(S,I)I + \eta S, \tag{5.1}$$

$$E_2 := \mathcal{D}_{0,w}^{\iota,\theta} I(t) - \rho - h(S,I)I + (\mu + \gamma + \xi)I, \tag{5.2}$$

$$E_3 := \mathcal{D}_{0,w}^{\iota,\theta} R(t) - \xi I - \eta S + \mu R, \tag{5.3}$$

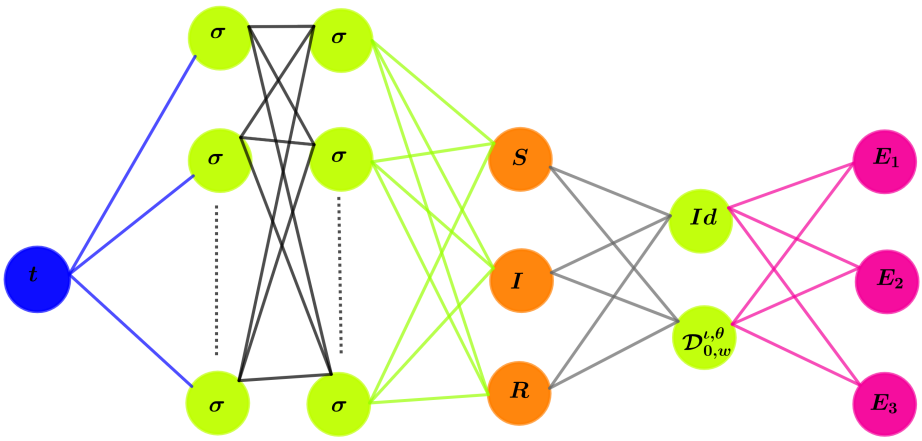

Figure 4: An example of the neural network method using PINNs.

Figure 4 provides a schematic illustration of the resultant PINNs for SIR. In this figure, "Id" denotes the identity operator and the differential operator "$\mathcal{D}^{\iota,\theta}_{0,w}$" is computed using automatic differentiation and can be thought of as an "activation operator". Moreover, the gradients of the loss function are back-propogated through the entire network to train the parameters using a gradient-based optimization algorithm. Specifically, we assume that the observables

$$C^M = \{S^p, I^p, R^p\}_{p=1}^M,$$

are noisy data of size M, that corresponds to the real-world data. Given such data, we are interested in inferring the latent (hidden) quantities $S(t), I(t)$ and $R(t)$. The shared parameters of the neural networks for S, I and R. In addition, the parameters $\{\Lambda, \Upsilon, \mu, \sigma, k, \eta, \rho, \gamma, \xi\}$ of the differential equation system (2.1) can be learned by minimizing the sum of squared errors loss function given by

$$\text{Loss} = \frac{1}{N_C}\sum_{j=1}^{N_C}\left(C^j - C^j_{pred}\right)^2 + \frac{1}{N_f}\sum_{k=1}^{N_f}\sum_{i=1}^{5}\left(E_i^k\right)^2.$$

Here, the first term corresponds to the training data $\left(t^j, C^j\right)$ for $j = 1 \dots N_C$, while the second term enforces the structure imposed by the system (2.1) at a finite set of measurement points whose number and locations are taken to be the same as the training data. It should be pointed out that the number and locations of the points on which we enforce the set of differential equations could be different from the actual training data. This procedure is described next by a PINNs algorithm in [14].

Let us consider a complete fractional problem of the following general form

$$\begin{aligned} \mathcal{D}^{\iota,\theta}_{0,w} C + \mathcal{L}[C;\Theta] = 0, \quad t \in [0,b], \\ C(0) = C_0, \end{aligned} \tag{5.4}$$

where $C(t) = \{S(t), I(t), R(t)\}$ is the latent solution, $\mathcal{L}[.;\Theta]$ is a nonlinear differential operator parametrized by $\Theta = \{\Lambda, \Upsilon, \mu, \sigma, k, \eta, \rho, \gamma, \xi\}$.

5.1. Simulating forward PINNs

For implementing the PINNs algorithm described earlier, we consider three hidden layers with 152 neurons each i.e. Neural Network layers $= [90, 90]$. With $N_C = 1000$ (by discretizing $t \in [0, 200]$). We

choose values of parameters provided from [16]. Choosing the parameters to be: $\Lambda = 5, \Upsilon = 1, \rho = 0, \sigma = 0.01, \gamma = 0.01, \mu = 0.01, \eta = 0.01, \xi = 0.01$, and $k = 0.1$. The output of the solution was treated as the input dataset to PINNs. The tolerance was chosen to be 0.01 for the Loss. The results are shown in Figures 5-7 for different values ι and θ. The numerical solution obtained from the PINNs validates the numerical data.

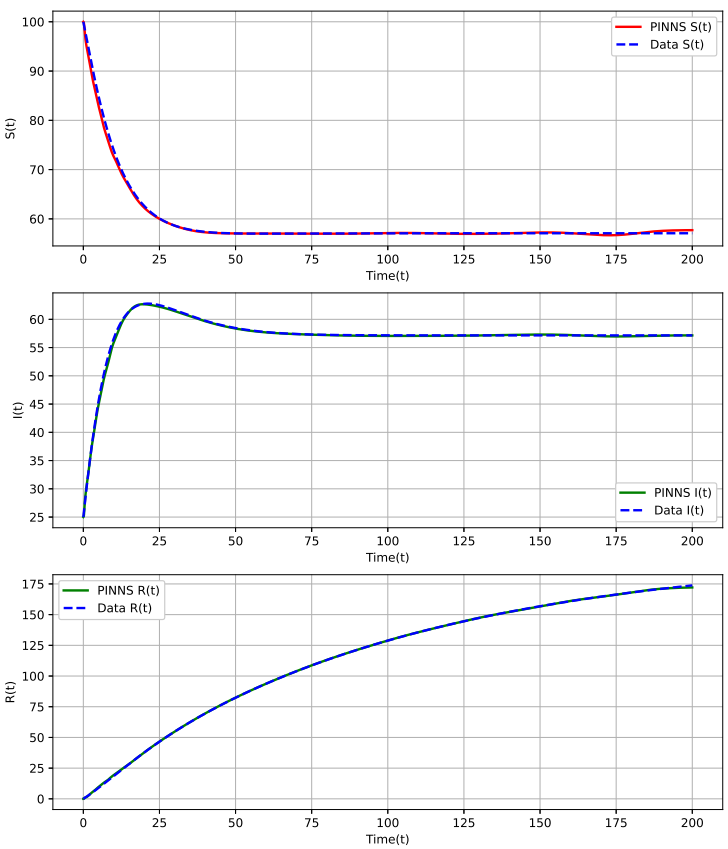

Figure 5: Numerical solution from forward PINNs validating data with $\iota = \theta = 1$.

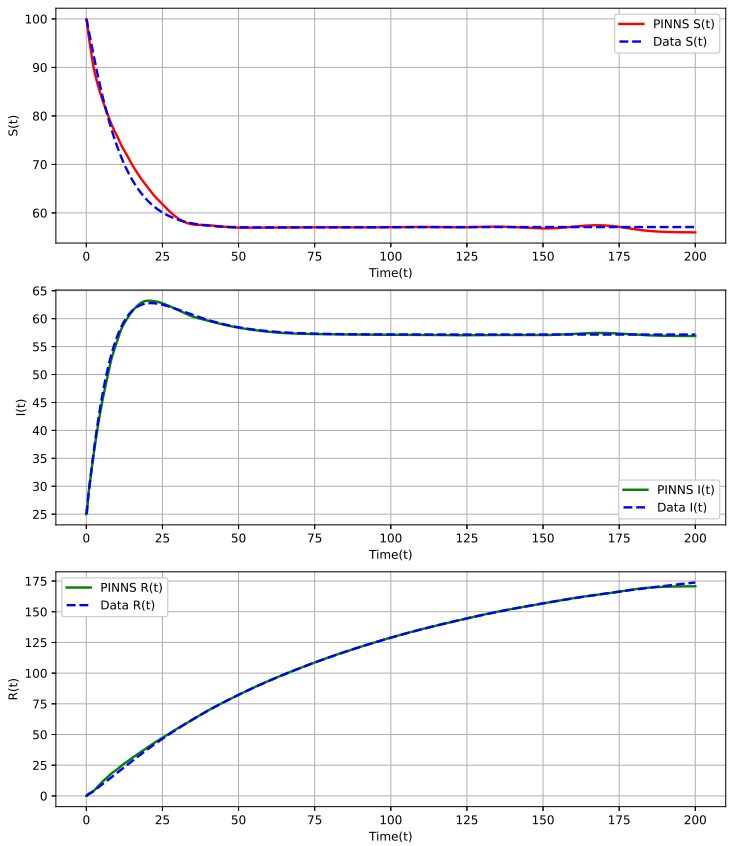

Figure 6: Numerical solution from forward PINNs validating data with $\iota = \theta = 0.5$.

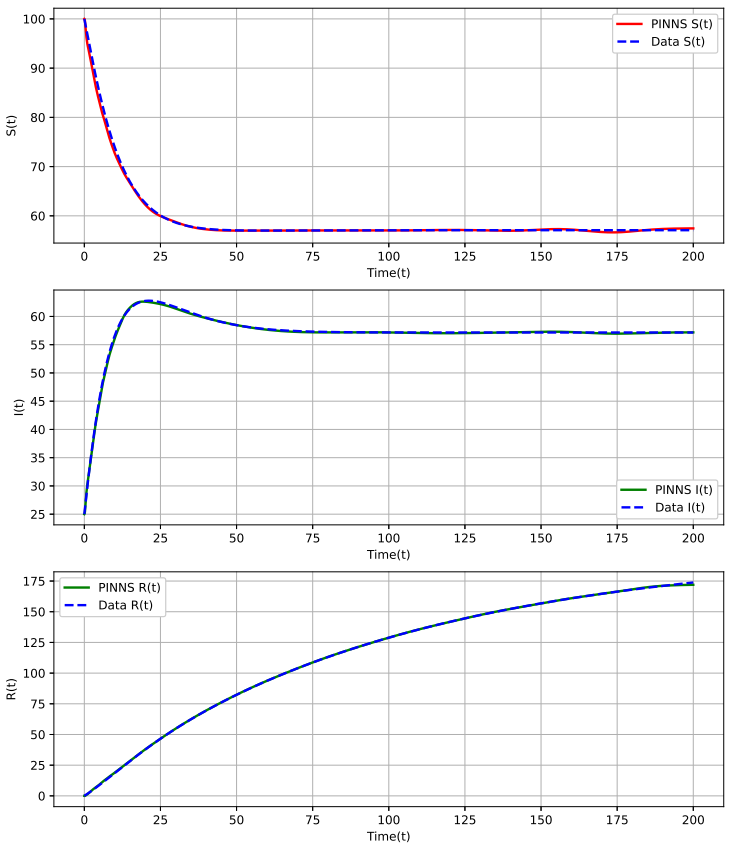

Figure 7: Numerical solution from forward PINNs validating data with $\iota = 0.5$ and $\theta = 0.8$.

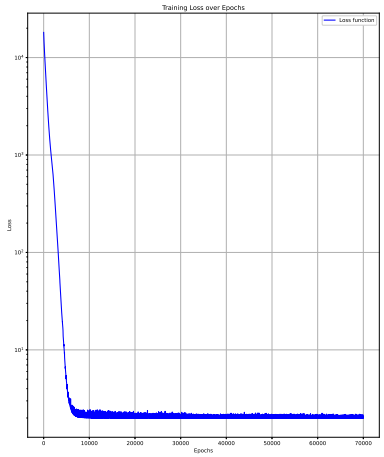

Figure 8: The loss function with $\iota = 0.5$ and $\theta = 0.8$.

Figures 9 to 11 illustrate the influence of the number of hidden layers on the accuracy of the solution approximation using PINNs.

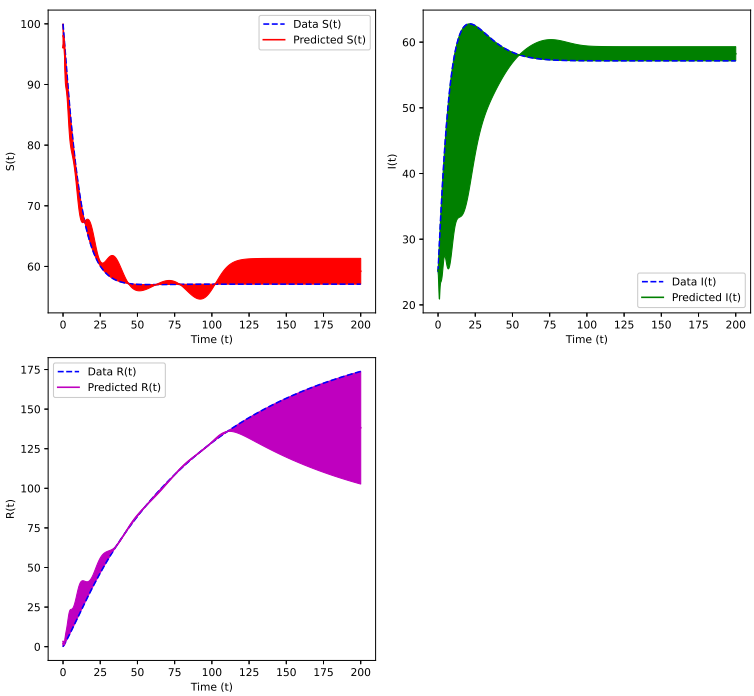

Figure 9: PINNs prediction with hidden dim= 20 and absolute error between data and prediction ($\iota = 0.5$ and $\theta = 0.8$).

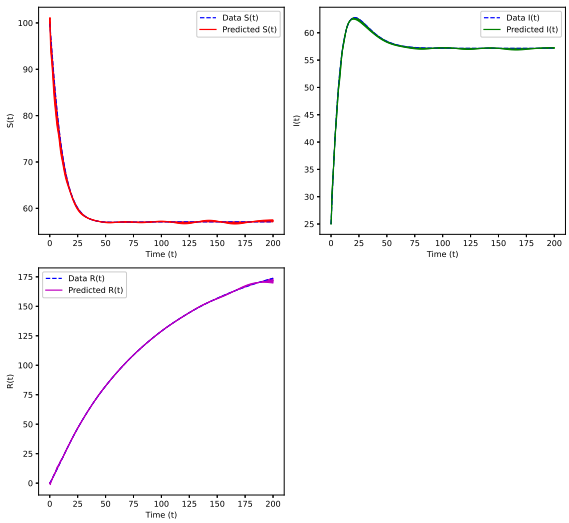

Figure 10: PINNs prediction with hidden dim= 50 and absolute error between data and prediction ($\iota = 0.5$ and $\theta = 0.8$).

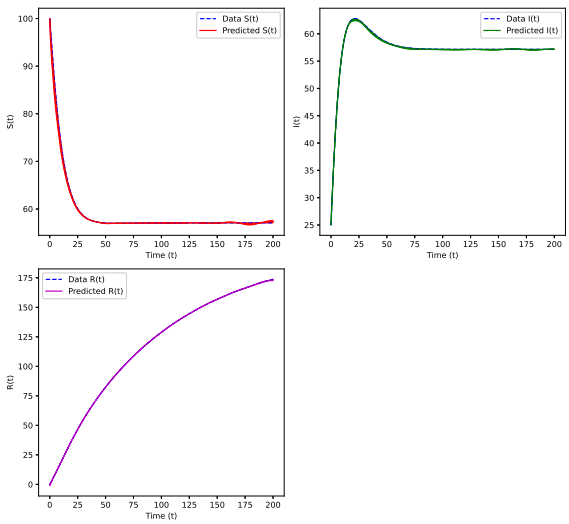

Figure 11: PINNs prediction with hidden dim= 100 and absolute error between data and prediction ($\iota = 0.5$ and $\theta = 0.8$).

Figures 9 to 11 show that increasing the number of hidden neurons (e.g. 20, 50, 100) in the PINN architecture has a significant impact on the quality of the approximation of the solutions of the fractional SIR system:
- For a small number of neurons (e.g. 20), the model has a limited representational capacity, which can lead to a coarse approximation of complex dynamics, especially in the rapid transition phases of infection.
- By increasing the size of the hidden layer to 50 neurons, we generally observe a better modeling of model

trends, with a significant reduction in prediction error on the $S(t)$, $I(t)$ and $R(t)$ compartments.
- With 100 neurons, the network has more flexibility to learn finer non-linear relationships, which often translates into more accurate predictions.

In short, the choice of the number of neurons is a compromise between complexity, computation time and accuracy.

6. Conclusion

In conclusion, this study has developed a fractional SIR model with the generalized Hattaf fractional derivative, incorporating a non-singular kernel, and integrated it into a PINNs framework. The analysis validates the existence, uniqueness, positivity, and boundedness of the solution, as well as proving the stability of the disease-free equilibrium in the sense of Mittag-Leffler. Moreover, the incorporation of PINNs offers a robust alternative to conventional numerical techniques for solving the SIR model. Our findings demonstrate that PINNs offer an effective approach for solving such systems and enhance our understanding of infectious disease dynamics, facilitating the estimation of fractional orders. On the other hand, the infection process in our model is described by a general incidence function where the infection rate is not dependent on time. However, the social distancing measures in the case of COVID-19 affect the infection rate of the virus, i.e., convert it to a time dependent function. Therefore, the improvement of our fractional model by taking into account the time-dependent infection rate will be addressed in our future research. In addition, we plan to integrate other generalized fractional and fractal-fractional derivatives, as introduced in [25,26,27], with Physics-Informed Neural Networks (PINNs) to analyze the dynamics of real-world phenomena

References

1. E. Kharazmi, M. Cai, X. Zheng, Z. Zhang, G. Lin and G. E. Karniadakis. Identifiability and predictability of integer and fractional-order epidemiological models using physics-informed neural networks. Nat Comput Sci, 1, 744-753, (2021).
2. J. Sirignano and K. Spiliopoulos. DGM: A deep learning algorithm for solving partial differential equations. Journal of computational physics, 375, 1339-1364, (2018).
3. L. Meng, X. Mao and G. E. Karniadakis. DeepXDE: A deep learning library for solving differential equations. SIAM review, 63(1), 208-228, (2021).
4. Y. Guo, X. Cao, B. Liu and M. Gao. Solving partial differential equations using deep learning and physical constraints. Applied Sciences, 10(17), 5917, (2020).
5. M. Raissi, Deep hidden physics models: Deep learning of nonlinear partial differential equations. Journal of machine learning research, 19(25), 1-24, (2018).
6. G. Pang, L. Lu and G. E. Karniadakis. fPINNs: Fractional physics-informed neural networks. SIAM Journal on Scientific Computing, 41(4), A2603-A2626, (2019).
7. H. Ren, X. Meng, R. Liu, J. Hou and Y. Yu. A class of improved fractional physics informed neural networks. Neurocomputing, 562, 126890, (2023).
8. S. Wang and G. Karniadakis. GMC-PINNs: A new general Monte Carlo PINNs method for solving fractional partial differential equations on irregular domains. Computer Methods in Applied Mechanics and Engineering, 429, 117189, (2024).
9. G. D. Barmparis, G. P. Tsironis. Physics-informed machine learning for the COVID-19 pandemic: Adherence to social distancing and short-term predictions for eight countries. Quantitative Biology, 10(2), 139-149, (2022).
10. C. Millevoi, D. Pasetto and M. Ferronato. A physics-informed neural network approach for compartmental epidemiological models. PLoS comput biol, 20(9), e1012387, (2024).
11. H. Hu, C.M. Kennedy, P.G. Kevrekidis, and H.-K. Zhang. A modified PINN approach for identifiable compartmental models in Epidemiology with Application to COVID-19. Viruses, 14, 2464, (2022).
12. H. Aghdaouia, A. A. Raezahb, M. Tiliouaa and Y. Sabbara. Exploring COVID-19 model with general fractional derivatives: novel physics-informed-neural-Networks approach for dynamics and order estimation. J. Math. Computer Sci, 36, 142-162, (2025).
13. S. Cai, Z. Wang, S. Wang , P. Perdikaris and G. E. Karniadakis. Physics-informed neural networks for heat transfer problems, J. Heat Transfer, 143, 060801, (2021).
14. L. Nguyen, M. Raissi, and P. Seshaiyer. Modeling, Analysis and physics informed neural network approaches for studying the dynamics of COVID-19 involving human-human and human-pathogen interaction. Comput. Math. Biophys, 10, 1-17, (2022) .

15. K. Hattaf, A new generalized definition of fractional derivative with non-singular kernel, Computation, 8, 1-9, (2020).

16. M. Semlali, K. Hattaf, M. Sadik and A El gourari. Stability analysis of a delayed COVID-19 transmission model involving immigration and vaccination. Commun. Math. Biol. Neurosci, 2023, 101, (2023).

17. M. Caputo and M. Fabrizio. A new definition of fractional derivative without singular kernel. Prog. Fract. Differ. Appl, 1, 73-85, (2015).

18. A. Atangana and D. Baleanu. New fractional derivatives with non-local and non-singular kernel: Theory and application to heat transfer model. Therm. Sci, 20, 763-769, (2016).

19. K. Hattaf, Stability of Fractional Differential Equations with new generalized Hattaf fractional derivative, Mathematical problems in Engineering, 2021, 1-7, (2021).

20. A. Taylor, D. Lay, Introduction to functional analysis wiley, New York, (1980).

21. K. Hattaf, On the Stability and Numerical Scheme of Fractional Differential Equations with Application to Biology, Computation, 10(6), 1-12, (2022).

22. M. Raissi and P. Seshaiyer. Application of local improvements to reduced-order models to sampling methods for non-linear PDEs with noise. International Journal of Computer Mathematics, 95(5), 870-880, (2018).

23. M. Raissi and G. Karniadakis, E. Hidden physics models: Machine learning of nonlinear partial differential equations. Journal of computational physics, 357, 125-141, (2018).

24. M. Raissi, P. Perdikaris and G.E. Karniadakis. Physics-informed neural networks: A deep learning framework for solving forward and inverse problems involving nonlinear partial differential equations. Journal of Computational Physics, 378, 686-707, (2019).

25. K. Hattaf. A new class of generalized fractal and fractal-fractional derivatives with non-singular kernels. Fractal Fract. 7(5), 395, (2023).

26. K. Hattaf. A new generalized class of fractional operators with weight and respect to another function. J. Fract. Calc. Nonlinear Syst, 5, 53–68, (2024).

27. K. Hattaf. A new mixed fractional derivative with applications in computational biology. Computation, 12(1), 7, (2024).

[1] *EMA Team, RST Laboratory, ESEFA, Ibnou zohr University of Agadir, Morocco.*

[2] *Equipe de Recherche en Modélisation et Enseignement des Mathématiques (ERMEM), Centre Régional des Métiers de l'Education et de la Formation (CRMEF), 20340 Derb Ghalef, Casablanca, Morocco.*

[3] *Laboratory of Analysis, Modeling and Simulation (LAMS), Faculty of Sciences Ben M'Scik, Hassan II University of Casablanca, P.O Box 7955 Sidi Othman, Casablanca, Morocco.*

E-mail address: moha.aitichou@gmail.com